Planetary and Space Science 175 (2019) 1–12

Contents lists available at ScienceDirect

Planetary and Space Science

journal homepage: www.elsevier.com/locate/pss

Investigating the effects of gamma radiation on selected chemicals for use in biosignature detection instruments on the surface of Jupiter's moon Europa

Caroline Freissinet [a,b,*], Maëva Millan [b,c], Daniel P. Glavin [b], Xiang Li [b], Andrej Grubisic [b], Jennifer E. Eigenbrode [b], Jennifer C. Stern [b], Jason P. Dworkin [b], Arnaud Buch [d], Cyril Szopa [a,e], Melissa A. Guzman [a], Martin A. Carts [f], Stephanie A. Getty [b], William B. Brinckerhoff [b]

[a] LATMOS-IPSL/CNRS, University of Versailles St Quentin, Guyancourt, France
[b] NASA Goddard Space Flight Center, Solar System Exploration Division, Greenbelt, MD, USA
[c] Georgetown University, Department of Biology, Washington, DC, USA
[d] Laboratoire de Génie des Procédés et Matériaux, Ecole CentraleSupelec, Gif-sur-Yvette, France
[e] Institut Universitaire de France, Paris, France
[f] NASA Goddard Space Flight Center, Radiation Effects Facility, Greenbelt, MD, USA

ARTICLE INFO

Keywords:
Europa
GC-MS
LD-MS
Radiation
Biosignatures
Chemical resistance

ABSTRACT

Jupiter's moon Europa is a prime target for the search for potential signs of life in the solar system. The Europa Lander Science Definition Team Report outlined investigations and measurement requirements on a future Europa Lander and has led us to consider application of powerful techniques such as pyrolysis and derivatization gas chromatography mass spectrometry (GC-MS) and laser desorption mass spectrometry (LD-MS) to elucidate the organic composition of near-surface ice and minerals. Definitive identification of chemical biosignatures using such techniques is strongly enabled by the use of various chemicals, such as perfluorotributylamine (PFTBA) for the MS calibration, α-cyano-hydroxycinnamic acid (CHCA) for matrix-assisted laser desorption and ionization (MALDI) and N,N-dimethylformamide dimethyl acetal (DMF-DMA), N-*tert*-butyldimethylsilyl-N-methyltrifluoroacetamide (MTBSTFA) and tetramethylammonium hydroxide (TMAH) for wet chemistry GC-MS protocols. The jovian radiation environment is known to represent a uniquely challenging risk to mission performance and lifetime, principally due to high radiation levels. To assess the potential ionizing radiation damage to these important chemicals, we tested their effectiveness following gamma radiation exposure doses up to the anticipated Europa Lander rating requirement of 300 krad(Si). The chemicals were sealed in glass ampules under vacuum (<10 mTorr), to reduce trapped oxygen gas, as the oxidation by O_2 may be enhanced in the presence of radiation. We report that all five chemicals exposed to total ionizing doses of 0, 150 and 300 krad(Si) maintained their full effectiveness, and no significant degradation was observed.

1. Introduction

Jupiter's moon Europa is a prime target for astrobiology; it may hold the clues to one of NASA's long-standing goals – to determine if there ever was or currently is life elsewhere in the solar system. Indeed, Europa very likely harbors a global, ~100 km deep, liquid water ocean in contact with a rocky layer of silicate (Kivelson et al., 2000). The ocean may be rich in the elements and energy needed for the emergence and survival of life (Chyba, 2000). Thus, Europa is a key body in the search for evidence of past or present life. The upcoming Europa Clipper space probe will provide a thorough analysis of this ocean world habitability potential during the planned 45 fly-bys of the mission. However, the Clipper payload is not specifically designed to detect potential molecular biosignatures. A future Europa lander that can directly sample and analyze the composition of the ice and other surface materials will be necessary to look for traces of life.

1.1. Instrumentation in development for Europa

The Europa Lander Science Definition Team (SDT) Report (Hand et al., 2017) outlines investigations and measurement requirements for a potential future Europa Lander. The measurement requirements have led

* Corresponding author. LATMOS, 11 boulevard d'Alembert, 78280, Guyancourt, France.
E-mail address: caroline.freissinet@latmos.ipsl.fr (C. Freissinet).

https://doi.org/10.1016/j.pss.2019.05.009
Received 25 October 2018; Received in revised form 13 May 2019; Accepted 17 May 2019
Available online 20 May 2019

us to consider pyrolysis and derivatization gas chromatography (GC-MS) and laser desorption mass spectrometry (LD-MS) techniques as the leading candidates for an *in situ* payload to elucidate both simple and complex organic composition of near-surface ice and other materials that could be in contact with liquid from a subsurface ocean (Li et al., 2016). However, the most thorough and definitive identification of chemical biosignatures using these techniques require the use of added compounds; Perfluorotributylamine (PFTBA) is used as a common mass calibration compound in gas-phase electron impact mass spectrometry, thanks to its high volatility and well-known mass spectrum that includes several clearly identifiable peaks (Creaser et al., 2000; Hübschmann, 2015). Most commonly used ions are from *m/z* 69 to *m/z* 502. PFTBA could be carried on the mission as an *in situ* calibrant.

For efficient ionization across a broad range of chemistries, matrix-assisted laser desorption and ionization (MALDI) holds promise for highly sensitive detection of non-volatile, complex biomolecules. MALDI analysis of large, non-volatile species, such as peptides, typically involves the protonating organic acid matrix α-cyano-hydroxycinnamic acid (CHCA), which provides significant enhancement effect in the ion generation. CHCA typically transfers protons onto the targeted organic molecules, converting large neutral molecules into protonated ions with little fragmentation. CHCA powder could be carried on the mission to be mixed with europan samples. In our current concept, CHCA powder will be carried in a separated container. During the experiment, the liquid europan sample would run through the CHCA container and partially dissolve the CHCA powder. Then, the sample and CHCA mixture would be deposited on a sample plate for subsequent analysis. This concept has been demonstrated recently by our group (Getty et al., 2017; Li, 2019).

Many compounds of astrobiological interest (*e.g.* amino acids, complex carboxylic acids, sugars, nucleobases) are too refractory and/or polar to be analyzed directly by GC-MS. Prior to GC separation and MS analysis, wet chemistry may be used to convert polar or non-volatile molecules into modified, volatile molecules amenable to GCMS for their detection, identification and chiral separation (Buch et al., 2009). Although the wet chemistry solvents have not yet been selected for a future Europa Lander instrument, we examined N,N-dimethylformamide dimethyl acetal (DMF-DMA), N-*tert*-Butyldimethylsilyl-N-methyltrifluoroacetamide (MTBSTFA) and tetramethylammonium hydroxide (TMAH), flight-proven derivatization and thermochemolysis reagents, each with different advantages and features.

DMF-DMA is a methylating reagent (Thenot and Horning, 1972; Thenot et al., 1972). It reacts at high temperature (>100 °C) with labile hydrogens of the target molecule, to form methyl esters. A key feature of DMF-DMA derivatization is that it preserves the chiral center of molecules, thus allowing an enantiomeric separation on an enantioselective GC column. DMF-DMA was studied and qualified for flight on two space-borne missions, Rosetta-Philae (Meierhenrich et al., 2001) and ExoMars 2020 (Freissinet et al., 2013). A typical reaction of DMF-DMA on an amino acid is shown in Fig. 1.

The MTBSTFA reaction replaces labile hydrogens of target molecules with a *tert*-butyldimethylsilyl group (Mawhinney and Madson, 1982). MTBSTFA is a versatile and sensitive derivatizing reagent (Buch et al., 2006; Schwenk et al., 1984). The reaction can happen between 75 °C and 300 °C. Although the derivatized molecules are of higher molecular weight, they become less polar, less reactive and thus more volatile, rendering them amenable to GC-MS (Fig. 1). MTBSTFA can be used by itself, however, adding a solvent and proton acceptor increases the reaction yield considerably. As such, dimethylformamide (DMF) was added as a solvent to MTBSTFA at a ratio of 1:4. MTBSTFA has a high derivatization yield, displays a great versatility and has already been successfully used in planetary exploration (Freissinet et al., 2015; Malespin et al., 2018).

Thermochemolysis using TMAH for terrestrial long chain carboxylic acid analysis was first reported in the 1960s (Robb and Westbroo, 1963). About 90% of published thermochemolysis applications have used TMAH (Challinor, 2001). In general, heat drives the reaction between acidic functional groups and an alkylating reagent to produce methyl ester and ether groups. Heat also assists in base-catalyzed cleavage of selected chemical bonds (*e.g.*, ester and ether bonds) and more limited thermal bond cleavage when temperatures are high enough for pyrolysis (>450 °C). TMAH dissolved in methanol at a ratio of 1:3 is a highly alkaline solution that induces hydrolysis and methylation reactions that begin by 270 °C. However, at experimental temperatures of 450–600 °C, TMAH induces thermochemolysis reactions (*i.e.*, combined pyrolysis and chemical methylation) that more completely release diverse molecules bound in macromolecules and make the liberated molecules detectable

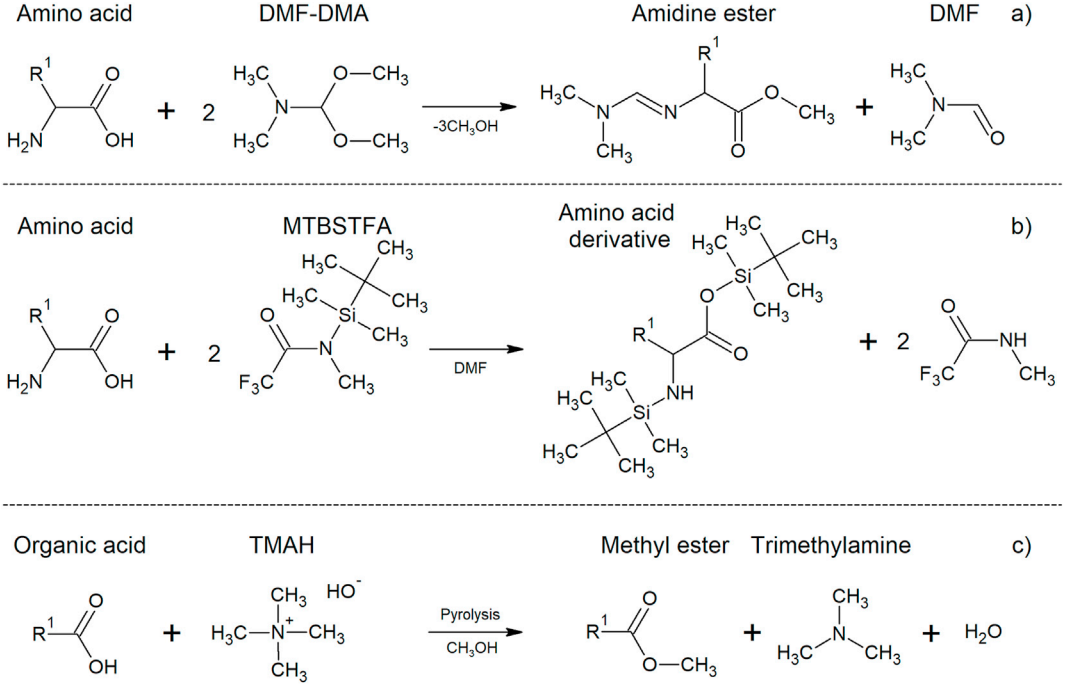

Fig. 1. (a) DMF-DMA reaction on a chiral amino acid, (b) MTBSTFA silylation on an amino acid, (c) TMAH methylation on a carboxylic acid.

via GC-MS using non-to mid-polar columns (Fig. 1) (Goesmann et al., 2017; Williams et al., 2019). TMAH experiments enables the detection and identification of carboxylic acids, particularly high molecular weight compounds from lipid membranes, such as fatty acids over 170 Da, as well as other structures released by hydrolysis of biomolecules and geomolecules (*e.g.*, carbohydrates, lignins, and amines from peptides and proteins after diagenesis). In contrast to MTBSTFA and DMF-DMA, TMAH is not sensitive to water and can be easily used in a water-rich environment without additional sample preparation.

1.2. Radiation environment at Europa

One of the most challenging hurdles of a Europa mission is the radiation environment. Radiation testing of some of these chemical species had been successfully performed in preparation for Mars Science Laboratory (MSL) mission. However, the total ionizing dose (TID) for a Europa Lander mission is expected to be ~50–100 times higher than for MSL, again raising the question of chemical agents robustness for *in situ* chemical analyses. GC-MS instruments have already been operated successfully several times in planetary exploration (Biemann et al., 1976; Ming et al., 2014; Niemann et al., 2002) and wet chemistry has proven to be reliable and efficient in the SAM instrument on the Curiosity rover (Freissinet et al., 2015). A combination of GC-MS, with wet chemistry, and LD-MS, is implemented on the Mars Organic Molecule Analyzer (MOMA) instrument (Goesmann et al., 2017) onboard the upcoming ExoMars rover mission. However, these techniques require a rigorous maturity assessment prior to their use in an ocean world environment such as Europa.

According to the Europa Lander SDT report (Hand et al., 2017), the jovian radiation environment represents a uniquely challenging risk to mission performance and lifetime. Based on the current mission design trajectories and GIRE-2p jovian radiation model, the lander would experience a TID of ~1.7 Mrad behind 100 mil Al (Si equivalent), primarily from electrons. The local lander radiation impact would be mitigated with a combination of hardened technology and shielding. To attenuate the expected lander dose to 150 krad(Si) (where rad(Si) unit corresponds to the adsorbed dose for silicon), most payload sensor and electronics hardware are housed in a radiation vault similar to that used on the Juno space probe, a strategy also planned for the Europa Clipper mission. All electronics within the vault must be rated to 300 krad(Si) in order to maintain a radiation design factor of two (RDF = 2). As such, exposure to ionizing radiation at these levels must be assessed for the reagent chemicals used in any *in situ* instruments (Creamer et al., 2018).

1.3. Simulating Europa Lander environmental conditions

The jovian environment is characterized by a combination of energetic electrons and atoms that would bombard the spacecraft. Protons are however expected to be substantially suppressed by spacecraft vault and instrument housing, and thus inflict minimum damage to the chemicals onboard. Energetic electrons are more difficult to shield and therefore considered to be the primary source of impacts. To assess the potential ionizing radiation damage to chemicals used in the proposed instruments for a Europa Lander mission, we performed gamma irradiation of a set of chemicals using the ^{60}Co source at the NASA Goddard Space Flight Center Radiation Effects Facility (GSFC REF). Exposure to gamma radiation was chosen to represent the driving case of absorbed radiation dose present during an actual mission, as the TID is considered sufficiently representative of the degradation potential, at 300 krad(Si), regardless of the radiation type.

Although the initial interaction with matter is different between gamma radiation (photons) and electrons, both initiate a shower of secondary electrons that precipitate ionization and activates numerous chemical reactions (Woo and Sandford, 2002). The basic mechanisms being similar during irradiation by both sources (Dole, 1972), the degradation is dependent upon the radiation doses regardless of the radiation type (Lee et al., 2007). Literature reports irradiation performed on many biological and chemical material with both gamma and electron type radiation, for comparison. The physical, chemical and biological properties were not different after irradiation with gamma ray or electron beam radiation source (Tallentire et al., 2010; Vieira and Del Mastro, 2002); significant distinguishing effects on chemical reactions conducting to physical effects could generally not be established at doses relevant to the ones expected for Europa Lander spacecraft (Choi et al., 2009). In some cases, though, slight differences were observed in biological properties or degradation patterns, when complex biological or chemical materials were subjected to gamma *vs.* electron radiation at high doses (Abdou et al., 2011; Gonzalez et al., 2012; Zenkiewicz et al., 2003), higher than the ones employed in this present study. Gamma and high-energy electrons differ in several subtle ways: dose rate, sample temperature rise, treatment duration and thus oxygen availability. The dose rate parameter, usually orders of magnitude higher with electrons, is difficult to hold equal in experiments comparing the gamma and electron irradiation effects.

It is known that the degradation of chemical and biological material caused by irradiation can be strongly associated with partial oxidation of the organic substances. The most reactive oxygen-derived radical is the hydroxyl radical (•OH) generated by ionizing radiation (Garrison, 1987). The presence of oxidants such as H_2O_2, H_2O or O_2 produces much larger amounts of •OH and other reactive species which participate in oxidative degradation from ionizing radiation (Abdou et al., 2011; Woo and Sandford, 2002). As the chemicals stored on a spacecraft would be nominally oxygen-free and because laboratory atmospheric oxygen and water vapor could produce increased radiative degradation or recombination, the chemicals were sealed under vacuum (<10 mTorr) in preparation for gamma exposure in this present investigation.

We report the results from the irradiation of three wet chemistry reagents, DMF-DMA, MTBSTFA and TMAH, an MS calibration compound, PFTBA, and an ionization promoter, MALDI matrix CHCA (Fig. 2) in powder form. Each compound was exposed to TIDs of 0, 150 and 300 krad(Si) of gamma-radiation, at room temperature, under vacuum (<10 mTorr).

2. Materials and methods

2.1. Materials

DMF-DMA (derivatization GC/GC-MS grade) sealed in individual

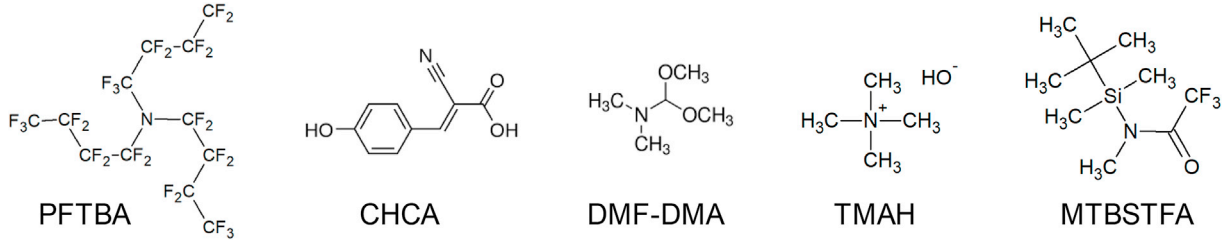

Fig. 2. Structural formulae of the five types of chemicals under investigation upon irradiation.

1 mL ampoules was purchased from Aldrich (P/N 394963). TMAH 25% w/w in methanol (stored under N_2), was purchased from Alfa Aesar in a 10 mL bottle (P/N 30833). MTBSTFA sealed in individual 1 mL ampoules (P/N 394882) was purchased from Sigma Aldrich (P/N 77626). The MS calibration reagent, perfluorotributylamine (PFTBA), was purchased from Sigma-Aldrich in a 25 mL bottle (P/N H5262). The MALDI matrix α-cyano-hydroxycinnamic acid (CHCA) was purchased from Sigma-Aldrich in a 1 g tube (P/N 70990).

2.2. Methods

2.2.1. Samples preparation and handling

For each of the chemicals, three sealed ampoules were prepared per exposure condition investigated: control samples (3 ampoules), 150 krad irradiation (3 ampoules) and 300 krad irradiation (3 ampoules). Borosilicate glass ampoules (13 mm × 100 mm) were heated in air at 500 °C overnight to remove any organic contamination. After filling the ampoules with each chemical (solid CHCA or liquid PFTBA, DMF-DMA, TMAH, and MTBSTFA), the individual ampoules were flame-sealed under vacuum (<10 mTorr) to minimize exposure of the chemicals to oxygen during the irradiation experiment and storage. The abundance of residual O_2 in the sealed ampules was not monitored in this investigation and may slightly vary due to the residual O_2 in the ampule and to further degassing of the sealed liquids. The DMF-DMA, MTBSTFA and TMAH test tubes were each filled with 0.5 mL solvent, the PFTBA tubes were filled with 0.1 mL, and 5–12 mg of solid powder was added to each CHCA tube. To avoid evaporation of the liquid samples under vacuum, the solvents were first frozen in liquid nitrogen prior to evacuating the test tube to <10 mTorr air on a vacuum line and flame-sealing. A total of 45 glass tubes were prepared, filled, sealed under vacuum and labeled. The DMF-DMA, MTBSTFA and TMAH ampoules were kept at 4 °C when not in use. PFTBA fluid and CHCA powder were kept sealed at room temperature at all times. All samples were prepared, irradiated and analyzed at NASA GSFC.

2.2.2. Irradiation

2.2.2.1. NASA Goddard space flight center (GSFC), radiation effect facility (REF). The gamma radiation exposure experiments were performed at the NASA GSFC REF which produces gamma rays at about 1 MeV. The irradiator is a panoramic type, in which the source radiates out into a room. As a consequence, the spectral purity is high compared to tunnel irradiators; if there is a photon energy dependence to the radiation effects this provides a more standardized 1 MeV result. Standard practice for this type of gamma irradiator is to irradiate targets within a Pb–Al enclosure. The outer Pb, layer, 1.575 mm thick, reduces the flux of low energy photons. The inner Al layer, also 1.575 mm thick, reduces the flux of low energy photons produced by the outer Pb layer. The net result of this filtering is to improve the spectrum by suppressing the lowest energy photons, which are present even in a panoramic irradiator.

Dosimetry at the GSFC REF is performed using open air ionization chambers (probes) designed for energy independence at the energies of interest. These are connected through triaxial cabling and dosimeter (electrometer-like) readout units, which are calibrated annually to NIST traceable settings by the manufacturer. Fluke 35040 Biomedical Advanced Therapy Dosimeters (readouts) and PTW 31015 0.03 cm^3 Pinpoint Chambers were used. The tolerance of dosimetry provided by the GSFC REF is ±10%. Desired exposure rate is achieved by adjusting a number of sources and the distance of the sources to the target. Iso-dose rate contours are not planar so the physical size of a target or group of targets affects the dose rate uniformity and the overall dosimetry tolerance.

2.2.2.2. Samples, dose rate and measurement units. Dose rate is measured within the filter box. Substitution dosimetry was used in this case. Exposure rate was measured and set (by adjusting filter box position) without the target materials present. The probes were removed for the actual irradiations and the total accumulated dose was calculated using exposure time. Three probe/cable/dosimeter systems were used in parallel. Prior to performing the actual dose rate measurements, the three probes were positioned together and irradiated in as uniform a field as possible in order to validate the system connections and operability.

The glass ampoules containing the samples were placed in cardboard test tube holders during gamma irradiation. The low density of cardboard makes it ideal for holding samples without attenuating the radiation. The control samples were stored under the same conditions, outside of the irradiation chamber. Two groups of samples were exposed, in the chamber in air at room temperature, one to 150 krad(Si) and another to 300 krad(Si). The two sample groups were arranged in planes orthogonal to the source material, each fitting within a 13 × 13 cm square, providing low spatial dose rate variation. They were held in a cardboard box, with the first rank (the 150 krad(Si) group) in front and the second rank (300 krad(Si)) separated by 0.6 cm. After the first round of irradiation (A), the first rank was removed for analysis. The second rank was moved forward for the second round of irradiation (B). Because these received slightly less dose during irradiation A, they were irradiated for slightly longer in irradiation B to achieve the correct final dose (300 krad(Si)). As expected, the borosilicate glass darkened with increasing gamma irradiation (Fig. 3). Table 1 gives the dose rates, times and incremental and total doses for the two groups.

Each different irradiation instance will have a specific, likely unique, spectrum of photon energies incident on the target, and therefore a specific correlation of exposure (roentgen, R) to absorbed dose (rad). GSFC REF equipment measures exposure, air kerma, in units of roentgen (R). The energy absorbed by a given material from an exposure is target material-dependent, and so will be the correlation for that material. Silicon (integrated circuits) is a prevalent target material irradiated in this type of facility. Correlation from exposure to rad(Si) is calculated by GSFC REF as 0.86565 rad(Si)·R^{-1}. Using these standards, 150 krad(Si) is 173.3 kR 300 krad(Si) is 346.6 kR.

2.2.3. DMF-DMA analyses

The analyses of DMF-DMA derivatives using both control and gamma-exposed DMF-DMA samples were performed on a Thermo Trace GC Ultra coupled to a quadrupole MS (Thermo ISQ II) with electron impact ionization at 70 eV. The example compounds used for experiments included D-phenylalanine (Sigma-Aldrich, ≥ 98%), L-phenylalanine (Sigma-Aldrich, ≥ 98%), D,L-alanine (Sigma-Aldrich, ≥ 99%), D,L-aspartic acid (Sigma-Aldrich, 99%), oxalic acid (Sigma-Aldrich, ≥ 99%), phthalic acid

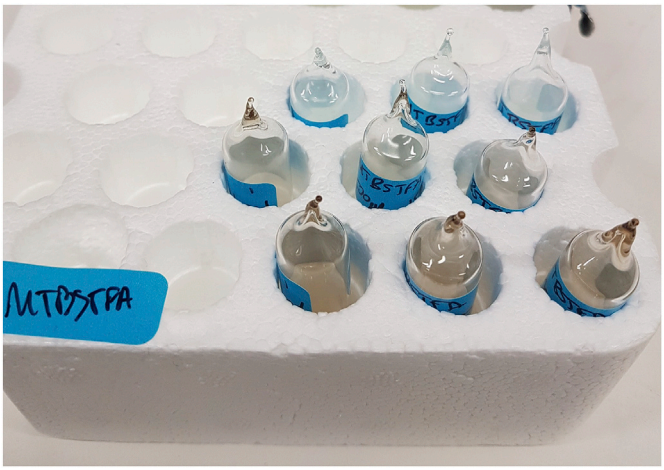

Fig. 3. The MTBSTFA flame-sealed ampoules in their styrofoam holder. Blanks (top row), 150 krad (middle row) and 300 krad (bottom row). A darkening of the borosilicate ampoule was observed after irradiation.

Table 1
Irradiation rates, times and doses.

Irradiation	First Rank Rate ($R{\cdot}min^{-1}$)	Second Rank Rate ($R{\cdot}min^{-1}$)	Irradiation time (h)	First Group Total Exp. (kR)	Second Group Incr. Exp. (kR)	Second Group Total Exp. (kR)	150 krad Group Total Dose (krad(Si))	300 krad Group Total Dose (krad(Si))
A	1590	1525	1.82	173.63	166.53	166.53	150.29	144.15
B	–	1590	1.89	–	180.31	346.84	–	300.22

(Sigma-Aldrich, ≥ 99.5%), (R,S)-2-methylsuccinic acid (Sigma-Aldrich, ≥ 99%) and uracil (Sigma-Aldrich, ≥ 99%). Stock solutions for each compound were prepared to a concentration of 10^{-2} mol L^{-1} dissolving each standard in Millipore Direct Q3 UV (18.2 MΩ, < 3 ppb total organic carbon) ultrapure water. A solution for testing the effectiveness of DMF-DMA derivatization was prepared from the stock solutions, as follows: 2 μL D-Phe + 2 μL L-Phe + 12 μL (D,L)-Ala + 4 μL DL-Asp + 16 μL oxalic acid + 4 μL phthtalic acid + 2 μL (R,S)-2-methylsuccinic acid + 10 μL uracil were added to a glass vial, and then dried under reduced pressure (~1 Torr) using a centrifugal evaporator at room temperature. 20 μL of DMF-DMA were then added to the dry residue, the vial was sealed with a cap and the derivatization reaction was performed at 140 °C for 3 min in a dry heating block (Freissinet et al., 2010). 1 μL of the standard methyl-nonanoate (10^{-2} mol L^{-1} in water) was added to the sample after the derivatization reaction. 1 μL of the derivatized solution was injected into the inlet of the GC set at 250 °C, with a 1 μL microsyringe. The GC conditions used were as follows: initial GC oven temperature of 70 °C, 3 °C·min^{-1} temperature ramp up to 190 °C and a hold at 190 °C for 1 min. The split ratio was 1:40 and the He flow rate was 1.2 mL min^{-1}. Helium purity was 99.9999%. The GC capillary column used was a fused silica J&W CP-Chirasil-Dex CB, 25 m × 0.25 mm × 0.25 μm, coiled in an 18 cm diameter cage. GC-MS analyses of one control, one 150 krad and one 300 krad irradiated DMF-DMA were performed, with a minimum of three replicates of each. GC-MS peak areas and the resolution of the enantiomeric separation (for chiral compounds) of the compounds derivatized with the control DMF-DMA (unexposed to radiation) were compared to the results obtained after derivatization with the gamma-exposed DMF-DMA reagents. Blank experiments (air-only GC injections) were run between DMF-DMA derivatized samples to monitor for potential cross-contamination. The microsyringe used for injecting the samples was rinsed three times with pure DMF between each analysis.

2.2.4. MTBSTFA analyses

Analyses of MTBSTFA derivatives were also performed on a Thermo Trace GC Ultra coupled to a quadrupole MS (Thermo ISQ II) with electron impact ionization (70 eV). The chemicals used for derivatization consisted of: D-phenylalanine (Sigma-Aldrich, ≥ 98%), L-phenylalanine (Sigma-Aldrich, ≥ 98%), D,L-alanine (Sigma-Aldrich, ≥ 99%), D,L-glutamic acid (Sigma-Aldrich, ≥ 98%), phthalic acid (Sigma-Aldrich, ≥ 99.5%), oxalic acid (Sigma-Aldrich, ≥ 99%) and cytosine (Sigma-Aldrich, ≥ 99%). A stock solution of each was made at 10^{-2} mol L^{-1} in Millipore Direct Q3 UV (18.2 MΩ, < 3 ppb total organic carbon) ultrapure water. The solution used for MTBSTFA derivatization was prepared from stock solutions as follows: 20 μL D-Phe + 20 μL L-Phe + 40 μL DL-Ala + 120 μL DL-Glu + 80 μL oxalic acid +40 μL phthalic acid +80 μL (R,S)-2-methylsuccinic acid + 160 μL cytosine were mixed together in a glass vial. 28 μL of the solution were dried under reduced pressure (~1 Torr) using a centrifugal evaporator at room temperature. 20 μL of MTBSTFA:DMF 4:1 were added to the dry residue. Note that only MTBSTFA was under investigation, and thus the DMF solvent was not irradiated. The DMF is not required for the silylation reaction to occur, and was only used as a solvent to improve MTBSTFA derivatization efficiency. The derivatization reaction was performed for 15 min at 75 °C in a dry heating block. After the reaction, 1 μL of methylnonanoate standard (10^{-2} mol L^{-1} in water) was added. 1 μL of the solution was injected in the GC-MS with a 1 μL microsyringe. The GC conditions were as follows: initial oven temperature of 70 °C held for 2 min, a 12 °C·min^{-1} temperature ramp up to 160 °C, immediately followed by a 10 °C·min^{-1} temperature ramp up to 200 °C and a final hold at that temperature for 9.5 min. The split ratio was 1:60 and the helium (99.9999% purity) flow rate was 1.2 mL min^{-1}. The capillary column used was a fused silica J&W CP-Chirasil-Dex CB GC Column, 25 m × 0.25 mm × 0.25 μm, coiled in a 18 cm diameter cage. GC-MS peak areas of the MTBSTFA derivatives from one control MTBSTFA were compared to the peak areas of the standards derivatized using the gamma-exposed MTBSTFA reagents (one 150 krad-exposed sample and one 300 krad-exposed sample). Three separate GC-MS analyses were conducted on each sample. Blank runs (air-only injection) were performed between samples to monitor cross-contamination. The microsyringe used for sample injections was rinsed five times with pure MTBSTFA between analyses.

2.2.5. TMAH analyses

Control (0 krad) and gamma irradiated (150 and 300 krad) TMAH samples were analyzed to determine if there was a relative change in its effectiveness as a thermal hydrolysis methylation reagent. A standardized mixture of carboxylic acids was analyzed with each TMAH test-reagent using a Frontier Autoshot-PY3030D pyrolyzer attached to an Agilent 7890A GC and 5975C inert XL mass spectrometer detector (MSD) with flame ionization detector (FID). The GC was fitted with a primary column Frontier Laboratory UA5-30M-0.25F (length 30 m, internal diameter 0.25 mm, and film thickness 0.25 μm) with 10% of the flow to the FID (column: 1.86 m length, internal diameter 0.15 mm, and no film). The inlet was fitted with a 40 mm diameter glass liner with 1 cm packing of glass wool.

The chemicals used for this set of tests included C_{14}, C_{19}, C_{22}, and C_{24} saturated carboxylic acids (Sigma-Aldrich, ≥ 98%). Stock solutions for each compound were prepared to a concentration of 0.2 g L^{-1} (0.54–0.88 mmol L^{-1} per compound) in dichloromethane (Fisher GC Resolv). These were mixed in equal parts for a test mixture. 10 μL of the mixture was added to an ashed steel pyrolysis cup and air dried. 5 μL TMAH-test reagent were added immediately before putting the cup in the pyrolysis apparatus. Once the pressure returned to the nominal operating value, the inlet was cooled to 0 °C. The sample was moved into the pyrolyzer oven at 40–45 °C at the start of the GC analysis. Once the system pressure stabilized and the pyrolyzer had been purged with 1 bar helium flowing at 11 mL min^{-1}, the oven/sample was ramped at 600 °C·min^{-1} to 600 °C, where it was held for 5 min while the inlet was cryogenically cooled at 0 °C, facilitated by liquid N_2 cooling, to trap volatiles on the glass wool in the inlet liner (no other adsorbent). The inlet cooling continued for an additional 2 min after pyrolyzer oven ramp ended to ensure trapping of analytes in the inlet, then ramped at 100 °C·min^{-1} to 300 °C and held for 0.3 min before returning to 250 °C for the duration of the GC run and to prevent excess septum bleed. Volatiles were split at a ratio of 10:1 and carried by a constant 1 mL min^{-1} flow of helium to the GC column. The GC oven program started at 40 °C and was held for 10.3 min to accommodate cryogenic trapping of analytes in the inlet. It was then heated at 20 °C·min^{-1} to 60 °C and held for 3 min to allow solvent to separate from analytes of interest. It was then ramped again at 20 °C·min^{-1} to 175 and then 15 °C·min^{-1} to 320 °C and held for 2 min. Total run time was 32 min plus a 5 min post run cleanup of all the columns.

After a 19 min solvent delay, the MSD was operated in combined scan and Single Ion Monitoring (SIM) modes. Scan mode monitored 33–550 *m/z* range with 2.82 scans·s^{-1}. SIM mode monitored *m/z* values (74,

87,143, 242, 312, 354, 382) with 100 ms dwell times. Masses were selected based on mass spectrum of expected carboxylic acid methyl ester products and were used to confirm their presence. The FID was operated with 50 mL min^{-1} H_2, 450 mL min^{-1} zero air, and 50 mL min^{-1} He flow. Relative quantitation was performed using FID signals that were corrected using column compensation of a blank run of the same method (*i.e.*, the blank background is automatically subtracted from the signal).

2.2.6. CHCA analyses

We compared the mass spectra of the CHCA powder by itself before and after gamma irradiation. In addition, diluted peptide standards (Angiotensin II human - Sigma Aldrich, ≥ 93%, HPLC grade, and His-Cys-Lys-Phe-Trp-Trp - Sigma Aldrich, ≥ 95%, HPLC grade) were also used to evaluate the MALDI effect of CHCA before and after the irradiation of the powder. Control and irradiated powdered CHCA samples were prepared by first dissolving in a 50:50 (v/v) (0.1% trifluoroacetic acid (TFA) in water):(acetonitrile) solution, yielding a CHCA concentration of 10 mg mL^{-1}. The peptide standard analytes were premixed with CHCA in the same solution. To analyze the samples, about 2 μL sample solution was drop-cast onto a highly polished ground stainless steel LD-MS target plate and dried in air before transferring into a commercial MALDI Time-Of-Flight (TOF) mass spectrometer (Bruker Autoflex Speed). The ion source of the commercial instrument was equipped with a Nd:YAG laser (355 nm, < 5 ns pulse) focused to a spot with approximate dimensions of 0.2 × 0.2 mm.

2.2.7. PFTBA analyses

PFTBA is commonly used as a wide mass range calibration compound in mass spectrometry, with a typical implementation relying on low flow rate (~pmol·s^{-1}) sampling of the PFTBA vapor from the headspace above the liquid PFTBA into a moderate pressure (~3 mTorr He) mass spectrometer ion source, as schematically depicted in Fig. 4. To understand whether radiation impacts the ability of PFTBA to serve as a mass range calibrant, we recreated the typical setup from off-the-shelf parts and pipetted ~0.5 mL of each of the 3 PFTBA liquid samples from their respective ampoules (0 krad, 150 krad, and 300 krad radiation exposure) into separate, pre-cleaned and baked (200 °C overnight) stainless steel containers (see inset to Fig. 4). Each of the containers was installed in the setup and headspace evacuated through the leak valve into the MS until stable high pressure was measured (~5 min), thus ensuring that the air had been displaced with PFTBA vapor continuously sourced from the liquid. This guaranteed that the PFTBA vapor was the dominant contributor of the efflux through the leak valve into the electron impact ion source of a MOMA prototype ion trap mass spectrometer (ITMS). The valve was then closed until only a small amount of PFTBA was being leaked into the ITMS as determined by the PFTBA ion signal level at set ionization source conditions. After the signal level had stabilized (~10 min), 1000 spectra, each with a typical 10 ms ionization time, were averaged and compared.

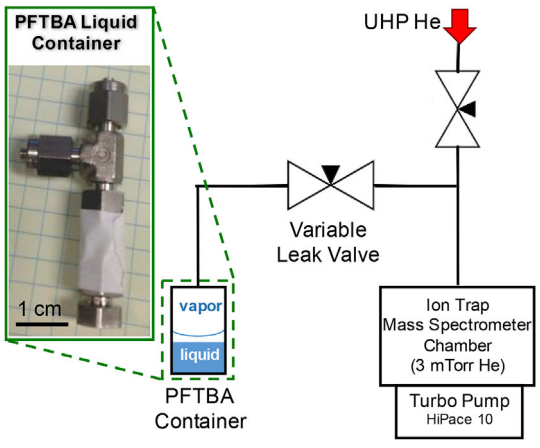

Fig. 4. Test setup for performing the evaluation of whether radiation impacts the ability of PFTBA to serve as the mass range calibrant in mass spectrometry. (left) Photo of the container utilized in lieu of the PFTBA calibration tank.

To eliminate significant sample cross-contamination between measurements, each time the sample reservoir was removed, the leak valve was purged with He and baked at 90 °C overnight to remove residual PFTBA. To confirm overall system cleanliness, efflux from a pre-baked, empty container was sampled by the mass spectrometer and PFTBA signature signal at mass-to-charge (m/z) ratio of 131 Da was ensured to be at least 100-fold weaker than when liquid was present.

3. Results and discussion

3.1. DMF-DMA

The molecules derivatized with DMF-DMA were chosen to include a variety of structures (aromatic and aliphatic compounds), a variety of chemical functions (amino acids, carboxylic acids, nucleobases), and the presence of chiral compounds for their enantiomeric separation. An example total ion chromatogram (TIC) from the GC-MS analyses showing separation of all of the derivatized compounds investigated for the DMF-DMA study is shown in Fig. 5. Although the derivatized molecule is the methyl ester of the initial molecule, we refer to the derivatized molecule as the initial molecule itself for simplicity. For each GC-MS run, the dead time was recorded using the air peak as the non-retained compound. The retention time of each compound relative to the dead time was also recorded. However, since the focus of this study was on the derivatization efficiency only (and not the GC column properties), the GC retention times relative to the dead times are not reported here. No additional peaks were observed between the control and the irradiated DMF-DMA (Fig. 5), at both 150 and 300 krad doses. This means no fragmentation or aggregation products of DMF-DMA caused by the gamma radiation exposure were observed.

For each compound investigated, the peak area of the methyl ester derivatized molecule was plotted relative to the area of the standard methyl-nonanoate (Fig. 6). The TIC area was used for most of the compounds, however for oxalic acid and alanine, the extracted ion chromatograms at m/z 59 and m/z 99, respectively, were used, due to some coelution of the TIC peaks with other DMF-DMA byproducts. No statistically significant changes were observed in the DMF-DMA derivatization yields on the variety of organic molecules investigated, after exposure to radiation, which indicates that the DMF-DMA itself was not degraded when exposed to gamma radiation up to a dose of 300 krad, and its reactivity was not impacted.

For the chiral compounds (R,S)-2-methylsuccinic acid, D,L-Alanine, D,L-Aspartic acid and D,L-phenylalanine, the resolution of enantiomeric separation R_s was also measured (Fig. 7). R_S is used to characterize the degree of separation of two peaks. Although this is more a property of the column and we do not expect to see a decrease in the resolution if DMF-DMA is still active, the enantiomeric separation is an important parameter for biosignatures detection and we decided to include this parameter in the study. Resolution depends on two parameters, the distance separating the two peaks (thermodynamics) and the width of each of the two peaks (kinetic factor). It is calculated as such (Eq. (1)): $R_s = 1.18\,(t_R^B - t_R^A)/(\omega_A + \omega_B)$, where t_R^A and t_R^B are the retention times of the first and second enantiomer, respectively, and ω_A and ω_B correspond to the peak width at half-height for the first and second enantiomer, respectively. Typically, a separation is considered baseline for $R_S > 1.5$, and the peaks are considered unseparated for $R_S < 0.6$. However, a high-number of theoretical plates on a column corresponding to high efficiency can allow baseline resolution at $1 < R_S < 1.5$ because of an increased sharpness of the peaks. The resolution of the enantiomeric peaks did not change before and after gamma irradiation of the DMF-DMA. The high error bar for alanine is explained by the coelution of the second alanine enantiomer (L-Ala) with

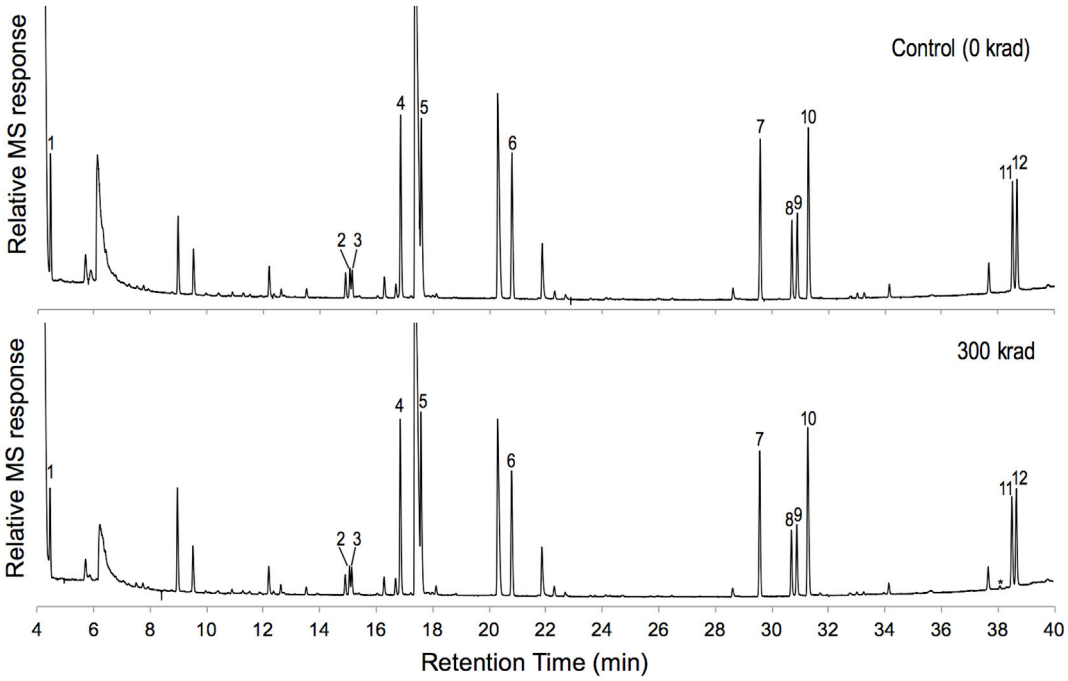

Fig. 5. Same scale chromatograms of the methyl esters of 1: oxalic acid, 2, 3: (R,S)-2-methylsuccinic acid, 4: D-alanine, 5: L-alanine, 6: methyl-nonanoate (standard), 7: phthalic acid, 8: D-aspartic acid, 9: L-aspartic acid, 10: uracil, 11: D-phenylalanine, 12: L-phenylalanine, obtained after derivatization with (top): control (non-irradiated) DMF-DMA, and (bottom): DMF-DMA gamma-irradiated at a 300 krad dose. The GC-MS data of the derivatization products obtained with DMF-DMA irradiated with a dose of 150 krad produced similar results (data not shown). *: instrument background.

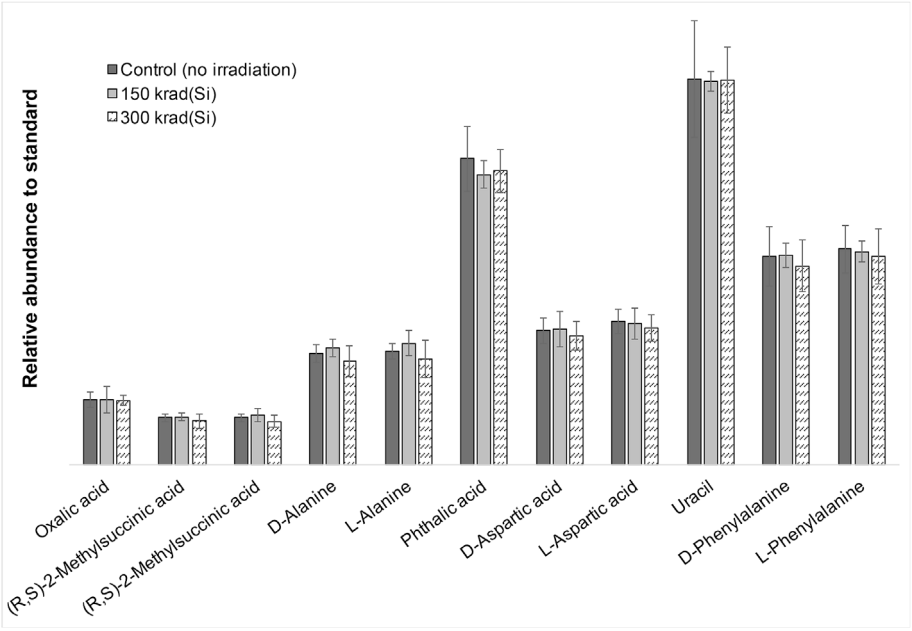

Fig. 6. Relative abundance of a variety of compounds derivatized with DMF-DMA, in their order of elution on the chromatogram. (R)- and (S)-2-methylsuccinic acid enantiomers are separated but their order of elution was not determined. DMF-DMA unexposed to gamma radiation (dark grey), exposed to a dose of 150 krad (light grey) and 300 krad (dashed). The error bars represent the standard deviation.

a byproduct of DMF-DMA (Fig. 5), which interfered with the retention of the molecule in the liquid phase of the column and widened the peak. DMF-DMA fully preserved its derivatization potential as well as its enantiomeric separation capability.

3.2. MTBSTFA

Derivatization with MTBSTFA was performed on aromatic and aliphatic compounds representing the three different chemical families of amino acids, carboxylic acids and a nucleobase. An example TIC chromatogram of the molecules targeted for the MTBSTFA study is shown in Fig. 8. Although the GC-MS peaks represent the *tert*-butyldimethylsilyl (*t*-BDMS) derivatives of the initial molecule, we refer to the derivatized molecule as the initial molecule for simplicity. Three additional peaks were observed in the GC-MS runs after gamma irradiation of the MTSBTFA at 150 krad and 300 krad doses compared to the non-

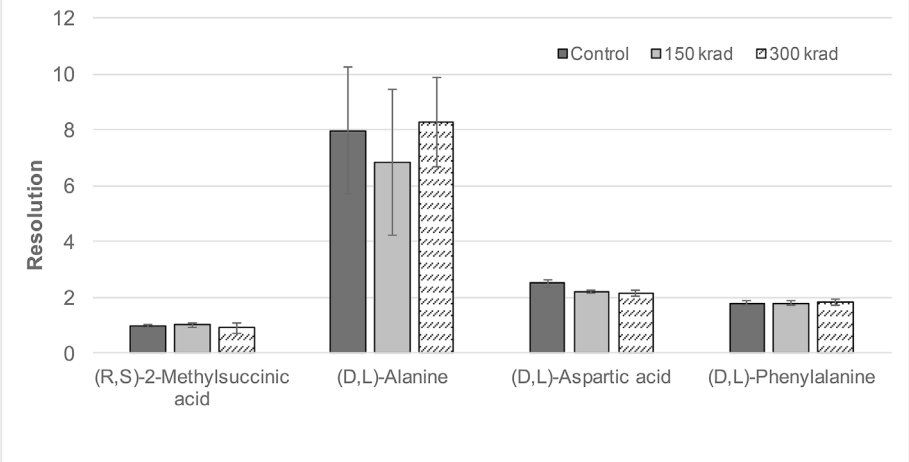

Fig. 7. Enantiomeric resolution (Eq. 1) of the chiral compounds under investigation (R,S)-2-methylsuccinic acid, DL-Alanine, DL-Aspartic acid and DL-phenylalanine). Derivatization with unexposed DMF-DMA (dark grey), DMF-DMA exposed to 150 krad (light grey) and 300 krad (dashed) of gamma radiation. The error bars represent the standard deviation.

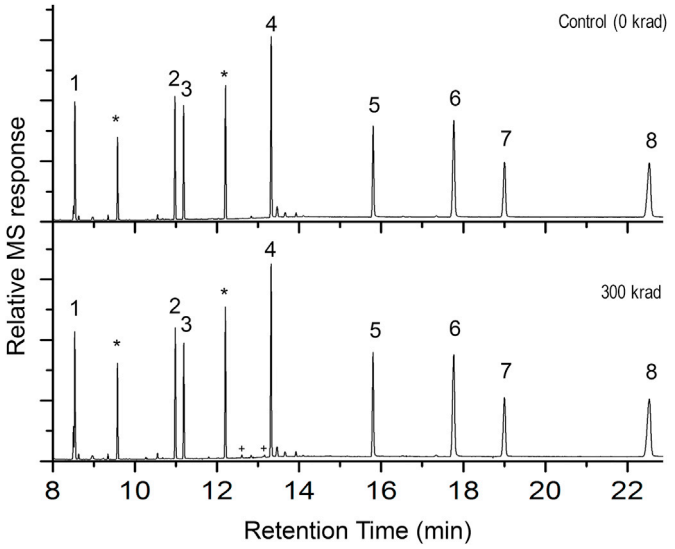

Fig. 8. Same scale chromatograms of selected *t*-BDMS derivatives after MTBSTFA:DMF derivatization for (top): non-irradiated MTBSTFA control and (bottom): MTBSTFA exposed to 300 krad gamma irradiation. 2: D, L-alanine, 3: oxalic acid, 4: methylsuccinic acid, 5: cytosine, 6: D, L-phenylalanine, 7: phthalic acid, 8: D, L-glutamic acid. 1 is the methyl-nonanoate used at the internal standard. The GC-MS data from the 150 krad exposed MTBSTFA sample produced similar results (data not shown). *MTBSTFA by-products. $^{+}$additional compounds observed after MTBSTFA irradiation and absent in non-irradiated control MTBSTFA sample.

irradiated control. Those peaks were detected at 12.6 min and two are co-eluted peaks at 13.1 min (Fig. 8). The compound eluting at 12.6 min is a degradation product of MTBSTFA. The compounds eluting at 13.1 min were not readily identified due to their co-elution. After the 300 krad MTBSTFA irradiation, the areas of these peaks, relative to the methyl-nonanoate standard peak areas, increased by a factor ~3 compared to the 150 krad dose, suggesting that all three peaks are degradation products of MTBSTFA induced by the irradiation process. Nevertheless, the net MTBSTFA degradation is quantitatively negligible and did not impact the derivatization efficiency for the organic compounds tested.

For each compound investigated, the area of the *t*-BDMS derivative was plotted relative to the area of the standard methyl-nonanoate (Fig. 9). The TIC was used for all derivatized compounds. For the methyl-nonanoate internal standard, the extracted ion chromatogram at *m/z* 87 was used due to the coelution with a known MTBSTFA by-product, *tert*-butyldimethylfluorosilane. The *tert*-butyldimethylfluorosilane mass spectrum does not show any ions at *m/z* 87. After irradiation of the MTBSTFA at 150 krad, the relative abundance of derivatized molecules to the standard decreased by 11% (D,L-Ala) to 18% (oxalic acid) with an average of 15% for all analyzed organic compounds (Fig. 9). For the MTBSTFA sample irradiated to 300 krad, the relative abundance of the derivatized molecules to the standard dropped an average of 4% relative to the control, taking into account all molecules (Fig. 9). The small decrease in abundance observed with the MTBSTFA irradiated to 300 krad(Si) falls within the standard error and is not considered a statistical loss of derivatization efficiency of the MTBSTFA reagent. The slight decrease in derivatization yield of the 150 krad exposed MTBSTFA falls within the standard deviation but not within the standard error. A Student *t*-test with 95% confidence demonstrated that although close to $p = 0.05$, the slight decrease was not statistically significant. It may be due to a higher abundance of trapped O_2 in the sealed vial used for the experiment, compared to the other two vials (control and 300 krad).

This hypothesis is supported by previous gamma radiation exposures of MTBSTFA sealed in air that showed a decrease in recovery of MTBSTFA derivatized amino acids after 6 krad exposure of the MTBSTFA relative to MTBSTFA that was not exposed. Earlier experiments on MTBSTFA and TMAH were performed to assure the relevance of MTBSTFA and TMAH in a martian environment for the Sample Analysis at Mars (SAM) wet chemistry experiment on the *Curiosity* rover (Mahaffy et al., 2012). The compounds were exposed to gamma radiation with total doses of 3 krad and 6 krad, twice the expected TID for the MSL mission. The irradiated fluids were then used to derivatize dry amino acid (for MTBSTFA) and carboxylic acid (for TMAH) standards that were subsequently analyzed by GC-MS. Ampoules of MTBSTFA (Sigma-Aldrich) were exposed to a 0, 3 and 6 krad dose using a ^{60}Co source. The ampoules were then opened, mixed with DMF in a 4:1 ratio (for MTBSTFA), and a standard dry mixture of amino acids was derivatized with the MTBSTFA:DMF. 98 ± 8% and 79 ± 12% of derivatized amino acids were recovered after 3 and 6 krad exposure, respectively, relative to an unexposed control MTBSTFA ampoule, suggesting some MTBSTFA degradation during gamma radiation exposure (Daniel P. Glavin, personal communication). Only two GC-MS measurements were performed. The significant decrease at 6 krad can be explained by the presence of O_2 in the ampoules. Indeed, the vendor's ampoules are routinely sealed under low humidity air, at atmospheric pressure (personal communication, Sigma-Aldrich technical support). Formation of oxidants from trapped O_2 during irradiation could have been responsible for the

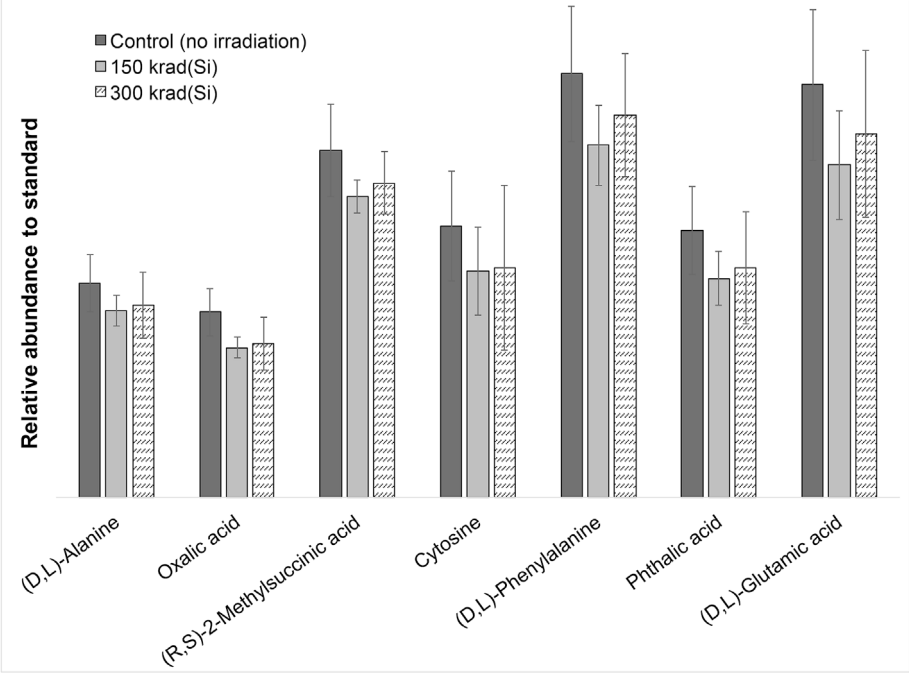

Fig. 9. Relative abundance of a variety of compounds derivatized with MTBSTFA:DMF. Unexposed (dark grey), exposed to 150 krad (light grey) and 300 krad (dashed) of gamma radiation. Only the MTBSTFA was irradiated. The error bars represent the standard deviation.

MTBSTFA degradation at the higher 6 krad dose. Irradiated TMAH tests showed similar reaction efficiencies (Jennifer L. Eigenbrode, personal communication). As such, wet chemistry reagents on future space probes would be sealed under oxygen-free conditions.

In conclusion, our data suggest that the MTBSTFA sealed under vacuum fully preserves its derivatization potential after exposure up to 300 krad.

3.3. TMAH

Thermochemolysis with TMAH was performed on long chain saturated carboxylic acids. An example chromatogram from the GC-FID analyses showing the methyl esters for the compounds investigated for the TMAH study is shown in Fig. 10. TMAH exposure to irradiation did not significantly impact the derivatization effectiveness for the organic compounds tested in this study. Additionally, TMAH, after gamma irradiation up to 300 krad(Si), did not display any detectable degradation products on the chromatograms.

Since the FID is a direct signal for total volatile organic carbon, and the background was automatically corrected, it was used for quantitation (Fig. 11). Peak areas calculated from the corresponding peaks in the FID chromatograph are used to gauge relative reaction efficiency. The identification of each carboxylic acid methyl ester derivative from the TMAH tests was confirmed using mass spectra. Results in Fig. 11 show little change in reaction efficiency for 150 and 300 krad irradiated TMAH compared to the control for C_{14}, C_{19}, and C_{22} saturated carboxylic acids, however not statistically significant. Average reaction efficiency relative to controls is 104–93%, with errors ranging up to 21% for the 300 krad C_{22} saturated carboxylic acid methyl ester result. The low values for the control and irradiated TMAH applied to C_{24} saturated carboxylic acid methyl ester may be the result of incomplete solvation of the carboxylic acid in dichloromethane.

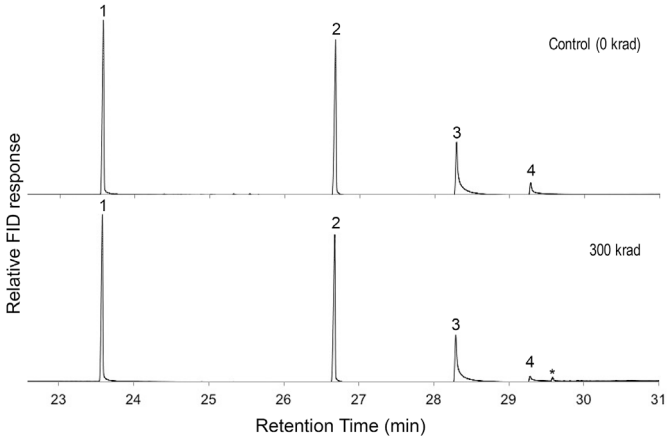

Fig. 10. Same scale chromatograms of selected methyl ester derivatives of saturated carboxylic acids after TMAH thermochemolysis for (top): non-irradiated TMAH control and (bottom): TMAH exposed to 300 krad gamma irradiation. 1: C_{14}, 2: C_{19}, 3: C_{22} and 4: C_{24} carboxylic acids. *: column bleeding.

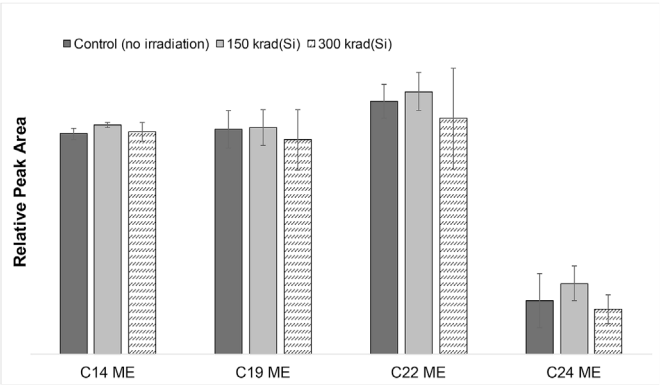

Fig. 11. Relative abundance of saturated carboxylic acid methyl esters produced by TMAH thermochemolysis. Unexposed (dark grey), exposed to 150 krad (light grey) and 300 krad (dashed) of gamma-radiation. The error bars represent the standard deviation.

3.4. CHCA powder

Fig. 12 (left) shows the comparison of mass spectrum of CHCA before irradiation with the spectra of irradiated CHCA under 150 krad and 300 krad of gamma irradiation. There is little difference amongst the three runs, regarding both signal intensity and type of peaks detected. This result indicates that the gamma irradiation did not cause chemical variation of the CHCA powder at the ~100 nM levels analyzed with LD-MS. Analysis of angiotensin II in CHCA showed comparable results: MALDI effectiveness was not measurably affected by the irradiation of CHCA. As shown in Fig. 12 (right), 2 µL of 10^{-7} mol L^{-1} angiotensin II mixed with non-irradiated or irradiated CHCA were detected under the exact same vacuum and laser conditions with comparable signal-to-noise ratio. Similar results were obtained with the His-Cys-Lys-Phe-Trp-Trp peptide.

MALDI-MS is designed primarily for detection of non-volatile, high molecular weight organic molecules and is not typically used for quantitative determination of concentrations. The collected ion signal intensity and stability can be influenced by several factors such as the laser output energy variation and surface roughness of the prepared samples. The spectra in Fig. 12 are comparable at the semi-quantitative level expected and targeted for MALDI. Although some minor variations in the mass spectrum pattern were observed in the 300 krad case, such as *m/z* 160 intensity increase (Fig. 12 bottom left panel), the main peaks of CHCA are comparable. In addition to the dose of radiation, the variations observed may also be caused by external factors such as variations in the laser energy and in the samples surface roughness. The experimental results have shown that the ability to detect diluted peptide by MALDI has been preserved, even after the CHCA has been radiated up to 300 krad. Therefore, we conclude that neither molecular structure of CHCA nor its protonation potential as a matrix has been significantly altered by radiation, suggesting that traditional MALDI methods are appropriate for application to large or complex organics at Europa.

3.5. PFTBA

PFTBA is used as a common mass calibration compound in electron impact MS, thanks to its well-known mass spectrum that includes several clearly identifiable peaks over a mass range commonly used from *m/z* 69 to m/z 502. The ratio between the peaks are also known and used to calibrate the MS response at low and high masses. Consequently, the integrity of the PFTBA molecule is critical for *in situ* investigation of organics investigation using MS. Our analysis of PFTBA aimed at understanding if Europa radiation levels would impact the composition of the PFTBA to the extent where mass and abundance calibration are impacted, if the masses or relative intensities of peaks change under radiation.

ITMS electron impact ionization spectra of the effluent sampled from

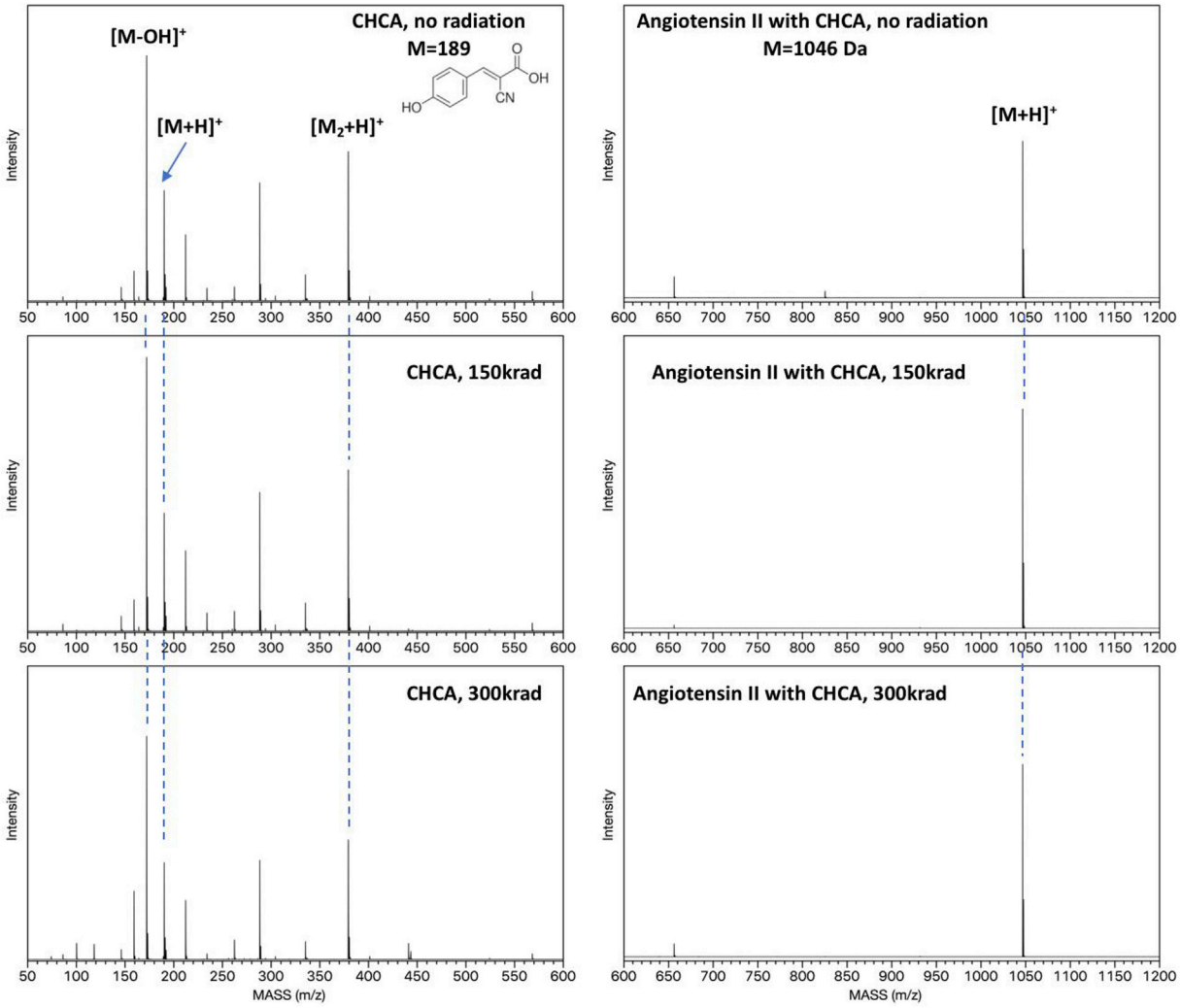

Fig. 12. Left panel: mass spectra of CHCA before irradiation compared to CHCA after 150 krad and 300 krad irradiation. Right panel: mass spectra of 10^{-7} mol L^{-1} angiotensin II mixed with control CHCA (top), 150 krad irradiated CHCA (middle) and 300 krad irradiated CHCA (bottom). The comparison spectra are collected under the same laser condition and plotted with the same signal intensity scale.

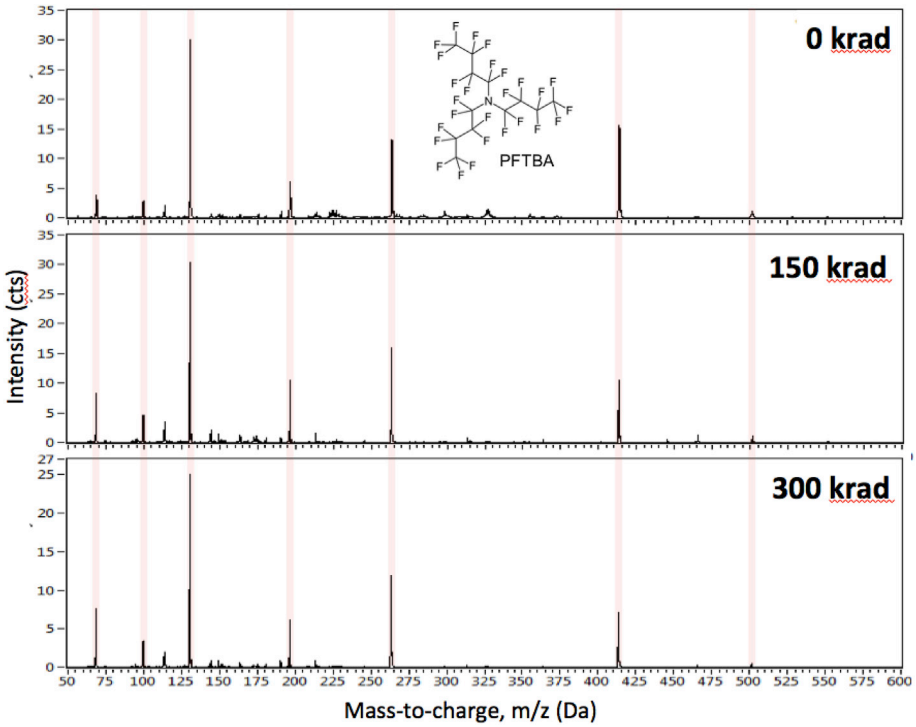

Fig. 13. Electron impact ionization ITMS spectra of the PFTBA vapors sampled from the headspace above the three PFTBA liquid samples and sent directly into the ion trap mass spectrometer indicate the composition of the vapor phase remains dominated by the PFTBA vapor even after irradiating the liquid, thus confirming PFTBA can serve as a high mass range calibrant for mass spectrometry up to at least 300 krad of total irradiation dose. Characteristic PFTBA mass fragments are highlighted.

the headspace above the PFTBA liquid are shown in Fig. 13 for the PFTBA procedural blank (0 krad) and the two irradiated samples (150 and 300 krad). The dominant mass spectrometric signature peaks of PFTBA ($m/z = 69$, 100, 131, 197, 264, 414 and 502 Da) are present for all 3 samples with mass spectra exhibiting essentially identical overall appearance and mass ratios even after a total dose of 300 krad. The results indicate that PFTBA remains the primary vapor phase constituent even after the liquid is exposed to 300 krad and can serve as a high mass range calibrant at mission-compatible radiation levels.

While every effort was made to ensure that the leak valve was opened to the same setting across sample measurements, irreproducibility in the flow rate at small flow rates prevented quantitative comparison of samples. It should be noted, however, that quantitative reproducibility in the mass flow rate is not required for PFTBA to serve as a mass calibrant in the most typical technical implementation, which was mimicked in our test setup. The flow rate, and thus the signal level, being exclusively dependent on the PFTBA vapor pressure, it would only be affected in the presence of large levels of volatile impurities. There is no evidence of impurities in mass spectral data, to account for a significant degradation of PFTBA. The results presented in Fig. 13 display similar mass spectra for the blank (0 krad irradiation) and irradiated samples, with a sufficiently preserved mass ratio between the runs and the absence of additional masses. This suggests preservation of the role of PFTBA compound, and an absence of volatile degradation products after irradiation up to 300 krad. The mass spectra thus indicate PFTBA continues to serve as a good mass calibrant even upon irradiation up to 300 krad.

4. Conclusion

To evaluate the potential ionizing radiation damage to chemicals used in techniques under consideration for a Europa Lander or other harsh radiation mission, we exposed five compounds critical to different GC-MS and LD-MS analyses to gamma radiation at TIDs of 0, 150 and 300 krad(Si). DMF-DMA, MTBSTFA, TMAH wet chemistry reagents remained fully functional after exposure to a TID of up to 300 krad. No or few degradation products of the chemicals were observed on the GC-MS or GC-FID runs. The resolution of enantiomeric separation of the chiral compounds was preserved with DMF-DMA derivatization. The three wet chemistry solvents should nevertheless be sealed under specific conditions to reduce trapped oxygen gas, as the solvent oxidation by O_2 may be enhanced in the presence of radiation. MALDI matrix CHCA retained its matrix effect and thus still facilitates the detection of high molecular weight organic molecules, such as peptides, after irradiation at 150 krad and 300 krad, without observable differences in the molecular signals. Lastly, the PFTBA investigation showed that this commonly-used MS calibration reagent would fully retain its mass calibration capability on such a remote mission. The heritage of calibration with this reagent is thus preserved. All five reagents investigated insure satisfying scientific capabilities upon gamma irradiation up to 300 krad. Use of CHCA, PFTBA and wet chemistry reagents from SAM and MOMA is therefore a plausible approach to maximize molecular detection and identification performance using GC-MS and LD-MS methods in astrobiological exploration of Europa.

Acknowledgments

The authors thank Megan C. Casey and Stephen K. Brown at the NASA GSFC REF for their fruitful discussion and help with the gamma irradiation. This work was funded by the NASA Concepts for Ocean worlds Life Detection Technology (COLDtech) Program. Declarations of interest: none.

Appendix A. Supplementary data

Supplementary data to this article can be found online at https://doi.org/10.1016/j.pss.2019.05.009.

References

Abdou, L.A.W., Hakeim, O.A., Mahmoud, M.S., El-Naggar, A.M., 2011. Comparative study between the efficiency of electron beam and gamma irradiation for treatment of dye solutions. Chem. Eng. J. 168 (2), 752–758.

Biemann, K., Oro, J., Toulmin, P., Orgel, L.E., Nier, A.O., Anderson, D.M., Simmonds, P.G., Flory, D., Diaz, A.V., Rushneck, D.R., Biller, J.A., 1976. Search for organic and volatile inorganic-compounds in 2 surface samples from chryse-planitia region of Mars. Science 194 (4260), 72–76.

Buch, A., Glavin, D.P., Sternberg, R., Szopa, C., Rodier, C., Navarro-Gonzalez, R., Raulin, F., Cabane, M., Mahaffy, P.R., 2006. A new extraction technique for in situ analyses of amino and carboxylic acids on Mars by gas chromatography mass spectrometry. Planet. Space Sci. 54 (15), 1592–1599.

Buch, A., Sternberg, R., Szopa, C., Freissinet, C., Garnier, C., Bekri, E.J., Rodier, C., Navarro-Gonzalez, R., Raulin, F., Cabane, M., Stambouli, A., Glavin, D.P., Mahaffy, P.R., 2009. Development of a gas chromatography compatible Sample Processing System (SPS) for the in-situ analysis of refractory organic matter in martian soil: preliminary results. Adv. Space Res. 43 (1), 143–151.

Challinor, J.M., 2001. Review: the development and applications of thermally assisted hydrolysis and methylation reactions. J. Anal. Appl. Pyrolysis 61 (1), 3-3-34.

Choi, J.-i., Kim, J.-H., Lee, K.-W., Song, B.-S., Yoon, Y., Byun, M.-W., Lee, J.-W., 2009. Comparison of gamma ray and electron beam irradiations on the degradation of carboxymethylcellulose. Korean J. Chem. Eng. 26 (6), 1825–1828.

Chyba, C.F., 2000. Energy for microbial life on Europa - a radiation-driven ecosystem on Jupiter's moon is not beyond the bounds of possibility. Nature 403 (6768), 381–382.

Creamer, J.S., Mora, M.F., Willis, P.A., 2018. Stability of reagents used for chiral amino acid analysis during spaceflight missions in high-radiation environments. Electrophoresis 39 (22), 2864–2871.

Creaser, C.S., West, S.K., Wilkins, J.P.G., 2000. Reactions of perfluorotri-n-butylamine fragment ions in the quadrupole ion trap: the origin of artefacts in the perfluorotri-n-butylamine calibration spectrum. Rapid Commun. Mass Spectrom. 14 (6), 538–540.

Dole, M., 1972. The Radiation Chemistry of Macromolecules. Academic Press, New York.

Freissinet, C., Buch, A., Sternberg, R., Szopa, C., Geffroy-Rodier, C., Jelinek, C., Stambouli, M., 2010. Search for evidence of life in space: analysis of enantiomeric organic molecules by N,N-dimethylformamide dimethylacetal derivative dependant Gas Chromatography–Mass Spectrometry. J. Chromatogr. A 1217, 731–740.

Freissinet, C., Buch, A., Szopa, C., Sternberg, R., 2013. Enantiomeric separation of volatile organics by gas chromatography for the in situ analysis of extraterrestrial materials: kinetics and thermodynamics investigation of various chiral stationary phases. J. Chromatogr. A 1306 (0), 59–71.

Freissinet, C., Glavin, D., Buch, A., Szopa, C., Kashyap, S., Franz, H., Eigenbrode, J.L., Brinckerhoff, W., Navarro-Gonzalez, R., Teinturier, S., Malespin, C.A., Prats, B., Mahaffy, P., 2015. First in situ wet chemistry experiment on Mars using the SAM instrument: MTBSTFA derivatization on a martian mudstone. In: Lunar and Planetary Science Conference.

Garrison, W.M., 1987. Reaction mechanisms in the radiolysis of peptides, polypeptides, and proteins. Chem. Rev. 87 (2), 381–398.

Getty, S.A., Elsila, J., Balvin, M., Brinckerhoff, W.B., Li, X., Grubisic, A., Cornish, T., Ferrance, J., Southard, A., 2017. Molecular analyzer for complex refractory organic-rich surfaces (MACROS). In: IEEE Aerospace Conference.

Goesmann, F., Brinckerhoff, W.B., Raulin, F., Goetz, W., Danell, R.M., Getty, S.A., Siljeström, S., Mißbach, H., Steininger, H., Arevalo, R.D., Buch, A., Freissinet, C., Grubisic, A., Meierhenrich, U.J., Pinnick, V.T., Stalport, F., Szopa, C., Vago, J.L., Lindner, R., Schulte, M.D., 2017. The Mars organic molecule analyzer (MOMA) instrument: characterization of organic material in martian sediments. Astrobiology 17 (7), 655-655-685.

Gonzalez, L.N., Arruda-Neto, J.D.T., Cotta, M.A., Carrer, H., Garcia, F., Silva, R.A.S., Moreau, A.L.D., Righi, H., Genofre, G.C., 2012. DNA fragmentation by gamma radiation and electron beams using atomic force microscopy. J. Biol. Phys. 38 (3), 531–542.

Hand, K.P., Murray, A.E., Garvin, J.B., Brinckerhoff, W.B., Christner, B.C., Edgett, K.S., Ehlmann, B.L., German, C.R., Hayes, A.G., Hoehler, T.M., Hörst, S.M., Lunine, J.I., Nealson, K.H., Paranicas, C., Schmidt, B.E., Smithe, D.E., Rhoden, A.R., Russell, M.J., Templeton, S.A., Willis, P.A., Yingst, R.A., Phillips, C.B., Cable, M.L., Craft, K.L., Hofmann, A.E., Nordheim, T.A., Pappalardo, R.T., a. t. P. E. Team, 2017. Report of the Europa Lander Science Definition Team. Posted Feb, 2017, URL as of the 13th of May 2019: : https://europa.nasa.gov/system/downloadable_items/50_Europa_Lander_SDT_Report_2016.pdf.

Hübschmann, H.-J., 2015. The Handbook of GC/MS Fundamentals and Applications. Wiley-VCH, p. 241. ISBN-10: 9783527334742.

Kivelson, M.G., Khurana, K.K., Russell, C.T., Volwerk, M., Walker, R.J., Zimmer, C., 2000. Galileo magnetometer measurements: a stronger case for a subsurface ocean at Europa". Science 289 (5483), 1340-1340-1343.

Lee, J.-W., Seo, J.-H., Kim, J.-H., Lee, S.-Y., Byun, M.-W., 2007. Comparison of the changes of the antigenicities of a hen's egg albumin by a gamma and an electron beam irradiation. Radiat. Phys. Chem. 76 (5), 879–885.

Li, X., 2019. In situ astrobiology investigation by molecular analyzer for complex refractory organic-rich surfaces (MACROS). In: AbSciCon Conference.

Li, X., Getty, S., Brinckerhoff, W., van Amerom, F.H.W., Danell, R., Pinnick, V., Arevalo, R., 2016. Development of the switchable ion polarity on linear ion trap mass spectrometry (LITMS). In: 47th Lunar and Planetary Science Conference.

Mahaffy, P.R., Webster, C.R., Cabane, M., Conrad, P.G., Coll, P., Atreya, S.K., Arvey, R., Barciniak, M., Benna, M., Bleacher, L., Brinckerhoff, W.B., Eigenbrode, J.L., Carignan, D., Cascia, M., Chalmers, R.A., Dworkin, J.P., Errigo, T., Everson, P., Franz, H., Farley, R., Feng, S., Frazier, G., Freissinet, C., Glavin, D.P., Harpold, D.N., Hawk, D., Holmes, V., Johnson, C.S., Jones, A., Jordan, P., Kellogg, J., Lewis, J., Lyness, E., Malespin, C.A., Martin, D.K., Maurer, J., McAdam, A.C., McLennan, D., Nolan, T.J., Noriega, M., Pavlov, A.A., Prats, B., Raaen, E., Sheinman, O., Sheppard, D., Smith, J., Stern, J.C., Tan, F., Trainer, M., Ming, D.W., Morris, R.V., Jones, J., Gundersen, C., Steele, A., Wray, J., Botta, O., Leshin, L.A., Owen, T., Battel, S., Jakosky, B.M., Manning, H., Squyres, S., Navarro-Gonzalez, R., McKay, C.P., Raulin, F., Sternberg, R., Buch, A., Sorensen, P., Kline-Schoder, R., Coscia, D., Szopa, C., Teinturier, S., Baffes, C., Feldman, J., Flesch, G., Forouhar, S., Garcia, R., Keymeulen, D., Woodward, S., Block, B.P., Arnett, K., Miller, R., Edmonson, C., Gorevan, S., Mumm, E., 2012. The sample analysis at Mars investigation and instrument suite. Space Sci. Rev. 170 (1–4), 401–478.

Malespin, C.A., Freissinet, C., Glavin, D.P., Mahaffy, P.R., Millan, M., Buch, A., Szopa, C., Teinturier, S., McAdam, A., Williams, R.H., Eigenbrode, J.L., Raaen, E., Dworkin, J.P., Navarro-Gonzalez, R., 2018. The first complete SAM wet chemistry experiment on Mars. In: Lunar and Planetary Science Conference.

Mawhinney, T.P., Madson, M.A., 1982. N-methyl-n-(tert-butyldimethylsily) trifluoroacetamide and related n-tert-butyldimethylsilyl amides as protective silyl donors. J. Org. Chem. 47 (17), 3336–3339.

Meierhenrich, U.J., Thiemann, W.H.P., Goesmann, F., Roll, R., Rosenbauer, H., 2001. Enantiomer separation of hydrocarbons in preparation for ROSETTA's "chirality-experiment. Chirality 13 (8), 454–457.

Ming, D.W., Archer, P.D., Glavin, D.P., Eigenbrode, J.L., Franz, H.B., Sutter, B., Brunner, A.E., Stern, J.C., Freissinet, C., McAdam, A.C., Mahaffy, P.R., Cabane, M., Coll, P., Campbell, J.L., Atreya, S.K., Niles, P.B., Bell, J.F., Bish, D.L., Brinckerhoff, W.B., Buch, A., Conrad, P.G., Des Marais, D.J., Ehlmann, B.L., Fairen, A.G., Farley, K., Flesch, G.J., Francois, P., Gellert, R., Grant, J.A., grotzinger, J.P., Gupta, S., Herkenhoff, K.E., Hurowitz, J.A., Leshin, L.A., Lewis, K.W., McLennan, S.M., Miller, K.E., Moersch, J.E., Morris, R.V., Navarro-Gonzalez, R., Pavlov, A.A., Perrett, G.M., Pradler, I., Squyres, S.W., Summons, R.E., Steele, A., Stopler, M., Sumner, D.Y., Szopa, C., Teinturier, S., Trainer, M.G., Treiman, A.H., Vaniman, D.T., Vasavada, A.R., Webster, C.R., Wray, J.J., Yingst, R.A., Team, M.S., 2014. Volatile and organic compositions of sedimentary rocks in yellowknife bay, Gale crater, Mars. Science 343 (6169).

Niemann, H.B., Atreya, S.K., Bauer, S.J., Biemann, K., Block, B., Carignan, G.R., Donahue, T.M., Frost, R.L., Gautier, D., Haberman, J.A., Harpold, D., Hunten, D.M., Israel, G., Lunine, J.I., Mauersberger, K., Owen, T.C., Raulin, F., Richards, J.E., Way, S.H., 2002. The gas chromatograph mass spectrometer for the Huygens probe. Space Sci. Rev. 104 (1–2), 553–591.

Robb, E.W., Westbroo, J., 1963. Preparation of methyl esters for gas liquid chromatography of acids by pyrolysis of tetramethylammonium salts. Anal. Chem. 35 (11), 1644–1647.

Schwenk, W.F., Berg, P.J., Beaufrere, B., Miles, J.M., Haymond, M.W., 1984. Use of tert-butyldimethylsilylation in the gas-chromatographic mass spectrometric analysis of physiologic compounds found in plasma using electron-impact ionization. Anal. Biochem. 141 (1), 101–109.

Tallentire, A., Miller, A., Helt-Hansen, J., 2010. A comparison of the microbicidal effectiveness of gamma rays and high and low energy electron radiations. Radiat. Phys. Chem. 79 (6), 701–704.

Thenot, J.P., Horning, E.C., 1972. Amino-acid N-dimethylaminomethylene alkyl esters - new derivatives for Gc and Gc-ms studies. Anal. Lett. 5 (8), 519–529.

Thenot, J.P., Stafford, M., Horning, E.C., Horning, M.G., 1972. Fatty-acid esterification with N,N-dimethylformamide dialkyl acetals for Gc analysis. Anal. Lett. 5 (4), 217–223.

Vieira, F.F., Del Mastro, N.L., 2002. Comparison of gamma-radiation and electron beam irradiation effects on gelatin. Radiat. Phys. Chem. 63 (3–6), 331–332.

Williams, A.J., Eigenbrode, J., Floyd, M., Wilhelm, M.B., O'Reilly, S., Johnson, S.S., Craft, K.L., Knudson, C.A., Andrejkovicova, S., Lewis, J.M.T., Buch, A., Glavin, D.P., Freissinet, C., Williams, R.H., Szopa, C., Millan, M., Summons, R.E., McAdam, A., Benison, K., Navarro-Gonzalez, R., Malespin, C., Mahaffy, P.R., 2019. Recovery of fatty acids from mineralogic Mars analogs by TMAH thermochemolysis for the sample analysis at Mars wet chemistry experiment on the curiosity rover. Astrobiology 19 (4), 522–546.

Woo, L., Sandford, C.L., 2002. Comparison of electron beam irradiation with gamma processing for medical packaging materials. Radiat. Phys. Chem. 63 (3–6), 845–850.

Zenkiewicz, M., Rauchfleisz, M., Czuprynska, J., 2003. Comparison of some oxidation effects in polyethylene film irradiated with electron beam or gamma rays. Radiat. Phys. Chem. 68 (5), 799–809.